Shamass, R., Cashell, K.A. Analysis of Stainless Steel-Concrete Composite Beams. Accepted for publication in the Journal of Constructional Steel Research, 2018.
https://www.sciencedirect.com/science/article/pii/S0143974X17312701

Analysis of Stainless Steel-Concrete Composite Beams

R. Shamass [a], K.A. Cashell [b]

[a] Division of Civil and Building Services Engineering, School of Build Environment and Architecture, London South Bank University, UK

[b] Dept of Civil and Environmental Engineering, Brunel University London, UK

Abstract

Stainless steel is increasingly popular in construction projects owing to its corrosion-resistance, excellent mechanical and physical properties and its aesthetic appearance. The current paper is concerned with the use of these materials in steel-concrete composite beams, which is an entirely new application. Current design codes for steel-concrete composite beams are based on elastic-perfectly plastic steel material behaviour neglecting strain hardening. Whilst this is a reasonable assumption for carbon steel, stainless steel is a very ductile material which offers significant levels of strain hardening prior to failure. Therefore, current design provisions typically result in inaccurate and overly-conservative strength predictions when applied to stainless steel composite beams. The current study presents for the first time, an analytical solution for predicting the plastic bending capacity of stainless steel–concrete composite beams with either full or partial shear connection. This method is a development of the continuous strength method (CSM). Since the analytical analysis requires complex mathematical solution, a simplified analytical solution is also proposed, utilising some of the assumptions in Eurocode 4. There are no tests currently available in the literature for stainless steel-concrete composite beams. Therefore, a finite-element model is developed and validated against a number of experimental results for composite beams made from normal or high strength carbon steel. The validated numerical model is then used to investigate the accuracy of the proposed analytical solution. It is concluded that both the full and simplified analytical solutions are reliable and the simplified analytical method provides a straight forward design tool for practical engineers.

Keywords: Stainless steel; composite beams; finite-element analysis, analytical analysis; continuous strength method; Eurocodes

1- Introduction

This paper is concerned with the behaviour of composite beams made from stainless steel. Steel-concrete composite members are widely used in the design and construction of modern structures such as bridges and high rise buildings. Depending on the degree of composite action, a significant increase in strength and stiffness performance is gained compared to a bare steel or concrete section. This results in savings not only in construction depth but also in terms of material consumption, which means also lower environmental impact and reduced energy consumption [1]. Composite beams which are subjected to positive bending (i.e. sagging) offer a particularly efficient use of the constituent materials. In this case, the steel section is subjected to tensile stresses whilst the concrete slab acts primarily in compression, thus utilising the favourable characteristics of each material.

It is generally desirable for plastic design that composite beams have a ductile cross-section, in which strain hardening develops in the lower flange before the collapse moment is reached [2]. However, for calculating the load-bearing capacity of composite beams, design codes such as Eurocode 4 [3] generally neglect strain hardening effects and employ a rigid-plastic analysis of the cross-section, thus providing conservative predictions of the capacity in many cases, particularly when ductile materials such as stainless steel are employed.

Stainless steel has been employed in construction since the 1920's, when the main usage was in building facades. Nowadays, stainless steel has become popular in a wide range of construction and load-bearing applications due to its excellent mechanical properties such as higher strength and ductility, better retention of strength and stiffness at high temperature [4] and excellent corrosion resistance properties, compared with carbon steel. Stainless steel does not require coatings to be applied, thus leading to life-cycle cost savings relative to carbon steel especially for offshore steel structures [5], as well as reducing maintenance and rehabilitation costs.

In recent years, stainless steel has been the subject of intensive research in order to provide useful, efficient and reliable design guidance for engineers. The vast majority of research into stainless steel has been focussed on bare steel elements. Researchers have

investigated the flexural behaviour of stainless steel columns subjected to compressive loading or combined compression and bending moment (e.g. [6-9]) and beams (e.g. [10-13]) as well as beams and columns under fire conditions (e.g. [14]).

The use of stainless steel in composite structures has hitherto received little attention from the engineering community and research studies have generally been limited to investigating the behaviour of concrete-filled stainless steel columns under different loading conditions using experimental and numerical analysis. Lam et al. [15] conducted experiments on the behaviour of axially loaded concrete-filled stainless steel elliptical sections made from normal and high strength concrete. Uy et al. [16] carried out experiments on concrete-filled stainless steel circular, square and rectangular sections of short and slender columns subjected to combined axial compression and bending moment. The behaviour of concrete-filled stainless steel circular and square tubular sections subjected to axial compression under fire conditions has also been studied through a series of experiments [17]. Moreover, nonlinear finite-element analysis was used to investigate the performance of concrete-filled stainless steel tubular columns of square, L-, T-, and + shape sections under axial compression or combined compression and bending moment [18, 19]. To date, there has been no research available in the public domain on traditional composite beams (i.e. a bare steel section connected to a concrete slab through shear connectors) using stainless steel. The following section describes the context in which these members are highly relevant in the current era.

2- Research significance and methodology

Stainless steel provides excellent mechanical properties, durability and fire resistance for structural applications, and can also reduce the maintenance costs required over the lifetime of a structure, compared with carbon steel. However, it is only in very recent years as the demands for more sustainable construction have been given higher prominence, that stainless steel has really become an attractive solution for certain applications. This growth in popularity has been accompanied by an increase in research although most of the studies to date has been limited to bare stainless steel elements as well as a few studies into concrete-filled stainless steel tubular sections. There has been no research, at least in the public domain, into the behaviour of composite beams using stainless steel elements acting together with a concrete slab. Nevertheless, in appropriate scenarios, this type of application could be ideal for stainless steel owing to

its ductility and durability. In particular, stainless steel composite beams could offer a very valuable solution in bridge applications, where harsh environments and difficult maintenance requirements pose an ever-increasing challenge to engineers. In such applications, the stainless section could be left exposed to the local environment without long-term maintenance requirements, thus reducing the life-cycle costs compared with carbon steel and also utilising the significant aesthetic appeal of stainless steel.

In addition to its durability credentials, stainless steel also has excellent mechanical properties especially in terms of ductility, toughness and resistance to fatigue, all of which are particularly relevant in bridges and structural applications in harsh environments. Stainless steels have greater ductility and capacity for work hardening compared with carbon steels. A ductile cross-section is necessary for plastic design and highly desirable for design in general so that warning is given before collapse and for moment redistribution to occur. According to current design codes, the plastic bending resistance of composite steel-concrete beams is determined by rigid-plastic theory in which the effective area of the steel member is stressed to its yield strength, neglecting any stain hardening effects in the steel. Although this is a reasonable assumption for carbon steel which has an elastic response, with a clearly defined yield point, followed by a yield plateau and a moderate degree of strain hardening, stainless steel has a nonlinear stress-strain response from very early stages as well as significant levels of strain hardening prior to failure. Therefore, the current design codes for composite carbon steel-concrete beams result in an incorrect plastic bending resistance when applied to members made from stainless steel.

In this context, the current study presents an analytical solution for estimating the bending resistance of composite stainless steel-concrete beams with either a full and partial shear connection, which are subjected to sagging moments. The proposed method is an adaptation of the continuous strength method (CSM), which has been developed and validated extensively in recent years for structural steel (e.g. [20]), structural stainless steel (e.g. [21]) and, more recently, for carbon steel-concrete composite beams [2]. Since there are no tests available on stainless steel-concrete composite beams, a nonlinear finite element model has been developed to study the response and investigate the accuracy of proposed analytical solution. Although the analytical solution yields accurate strength predictions, it requires complex mathematical solution. Therefore, a simplified analytical solution is also proposed, utilising some of the assumptions of Eurocode 4 [3].

3- The continuous strength method (CSM)

The continuous strength method (CSM) is a relatively recent approach for calculating the cross-sectional resistance of metallic members using two key components: (1) a base curve which defines the continuous relationship between compressive local buckling strain at the ultimate load and the cross-section slenderness and (2) a material model that allows for the stain hardening. Gardner and Nethercot [21] originally proposed the design method for stainless steel hollow sections loaded in compression, bending or combined compression and bending. The design method was further extended to calculate the cross-sectional compression and bending resistance of other metallic materials such as aluminium and high strength steel [20] as well as open stainless steel cross-sections subjected to various types of loading [22]. It was found that the method provides more accurate predictions of the cross-sectional resistance compared with those obtained using the Eurocode 3 [23] and ASCE [24] design codes. In 2008, the term "continuous strength method" was introduced, based on a continuous relationship between (inelastic) local buckling and a rational exploitation of strain hardening [25]. Earlier versions of the CSM used the Ramberg-Osgood material model for stainless steel which resulted in a very complex solution procedure. In later developments, a bi-linear, elastic, linear hardening material model was introduced to the method [26] before a more detailed quad-linear material model was included which accounts for both the length of yield plateau and the strain hardening behaviour of hot-rolled structural steel [2]. These modifications make the CSM more straightforward and easy to apply in exploiting the benefits of strain hardening. Furthermore, the CSM method was recently extended to incorporate composite construction for carbon steel-concrete beams under sagging bending moment, accounting for strain hardening in the steel element [2]. This proposed application of the method was shown to provide a more accurate prediction of the cross-sectional capacity compared with Eurocode 4 [3].

4- Analytical model for composite beams with stainless steel

4.1-General

Stainless steel is usually divided into five different families in accordance with the chemical composition, including the austenitic, ferritic, martensitic, precipitation-hardening and duplex grades. Each group offers different mechanical, physical and

chemical properties. However, the excellent strength, stiffness, ductility and durability properties of the austenitic and duplex grades make these the most common in structural applications, with the ferritic grades also being used in appropriate applications.

Stainless steel exhibits a very different constitutive response compared with carbon steel. Whereas carbon steel has a clear yield point, and relatively little strain hardening thereafter, stainless steel has a predominantly nonlinear stress-strain relationship even before yielding (see Fig. 1) with significant strain hardening in the post-yield range. In the absence of a clearly defined yield point, the stress at an offset to the 0.2% plastic strain, i.e. the 0.2% proof strength ($\sigma_{0.2}$), is typically used to define the yield stress for stainless steels. This is determined by drawing a line with a slope equal to the elastic modulus (E) between the 0.2% strain on the x-axis and the stress-strain curve. The ultimate tensile strength (σ_u) is typically around 500-700 N/mm^2 for austenitic stainless steels and 600-1000 N/mm^2 for the duplex grades (including hot and cold rolled material) [27]. In terms of ductility, the most common austenitic and duplex grades have a fracture strain (ε_u) of around 40-60% and 20-30%, respectively, compared to around 20-25% for carbon steel. It has been shown [28] that before yielding occurs, the stress-strain response can be idealised using the following relationship proposed by Ramberg-Osgood [29] and modified by Hill [30]:

$$\varepsilon = \frac{\sigma}{E} + 0.002\left(\frac{\sigma}{\sigma_{0.2}}\right)^n \tag{1}$$

where n is a strain hardening exponent. Beyond yield, the following expression proposed by Mirambell and Real [31] and Rasmussen [28] can be applied:

$$\varepsilon = \varepsilon_{0.2} + \frac{\sigma - \sigma_{0.2}}{E_2} + \varepsilon_{up}^{*}\left(\frac{\sigma - \sigma_{0.2}}{\sigma_u - \sigma_{0.2}}\right)^m \quad \text{where } \varepsilon_{up}^{*} = \varepsilon_u - \varepsilon_{0.2} - \frac{\sigma_u - \sigma_{0.2}}{E_2} \tag{2}$$

where $\varepsilon_{0.2}$ is the total 0.2% strain corresponding to $\sigma_{0.2}$ and m is a strain hardening coefficient. In the following sub-sections, the material models discussed herein are used to develop both a full and simplified analytical model, based on the continuous strength method approach, for stainless steel-concrete composite beams with full and partial shear connection.

4.2- Full shear connection

4.2.1- Basic assumptions in the full analytical model

For composite beams with full shear connection, where the shear connection deformability is very small, a single plastic neutral axis (NA) exists. The position of the neutral axis and the plastic bending moment capacity can be identified by applying the equilibrium of internal forces equations to the cross-section. The full analytical model developed in this section is based on the following assumptions:

- The plastic neutral axis is located within the concrete slab. Hence, the compressive force in the concrete is larger than the tensile force in the steel element. This case is very common and desirable in composite beams to avoid any local buckling in the steel member.
- The slip that occurs between the steel section and the concrete slab is assumed to be negligible and therefore is ignored and the strain distribution over the composite cross section is linear with constant curvature κ.
- Any reinforcement in the concrete slab is ignored in the calculations.

Although the models defined in this paper are presented in the context of composite beams made using stainless steel, the expressions are equally relevant and applicable to traditional carbon steel composite members, with an appropriate material model.

4.2.2- Full analytical expressions to determine the bending resistance

The full-range stress-strain relationship for stainless steel illustrated in the literature (e.g. [28]) typically describes the strain as an explicit function of stress. However, in order to use the CSM in conjunction with an accurate material law for stainless steel, it is necessary to obtain the stress as an explicit function of strain. Abdella [32] proposed an approximate inversion relationship with the stress (σ) expressed as an explicit function of strain (ε), as follows:

$$\sigma_1(\varepsilon) = \sigma_{0.2}\frac{r\left(\frac{\varepsilon}{\varepsilon_{0.2}}\right)}{1+(r-1)\left(\frac{\varepsilon}{\varepsilon_{0.2}}\right)^{p}} \qquad \text{for} \quad \varepsilon \leq \varepsilon_{0.2} \tag{3}$$

$$\sigma_2(\varepsilon) = \sigma_{0.2}\left[1+\frac{r_2\left[\frac{\varepsilon}{\varepsilon_{0.2}}-1\right]}{1+(r^*-1)\left(\frac{\frac{\varepsilon}{\varepsilon_{0.2}}-1}{\frac{\varepsilon_u}{\varepsilon_{0.2}}-1}\right)^{p^*}}\right] \qquad \text{for } \varepsilon > \varepsilon_{0.2} \tag{4}$$

where the material parameters are:

$$\varepsilon_{0.2} = \frac{\sigma_{0.2}}{E} + 0.002 \qquad\qquad r = \frac{E\,\varepsilon_{0.2}}{\sigma_{0.2}}$$

$$E_2 = \frac{E}{1 + 0.002\, n/e} \qquad p = r\frac{1 - r_2}{r - 1}$$

$$e = \frac{\sigma_{0.2}}{E} \qquad m = 1 + 3.5\frac{\sigma_{0.2}}{\sigma_u}$$

$$\sigma_u = \sigma_{0.2}\frac{1 - 0.0375(n - 5)}{0.2 + 185e} \qquad E_u = \frac{E_2}{1 + (r^* - 1)m}$$

$$r_2 = \frac{E_2\, \varepsilon_{0.2}}{\sigma_{0.2}} \qquad r_u = \frac{E_u(\varepsilon_u - \varepsilon_{0.2})}{\sigma_u - \sigma_{0.2}}$$

$$\varepsilon_u = \min(1 - \frac{\sigma_{0.2}}{\sigma_u}, A) \qquad p^* = r^*\frac{1 - r_u}{r^* - 1}$$

$$r^* = \frac{E_2(\varepsilon_u - \varepsilon_{0.2})}{\sigma_u - \sigma_{0.2}}$$

In these expressions, ε_u is the ultimate tensile strain, A is the stainless steel elongation, E_2 and E_u are the slope of the stress-strain curve at $\varepsilon_{0.2}$ and ε_u, respectively, and r, r_2, r*, r_u, p, p* and m are parameters that need to be determined.

Fig. 2 shows the strain distribution through the depth of the cross-section for composite beams with a full shear connection together with the corresponding stress distribution obtained using the material model presented in Eqs. 3 and 4. In this figure, ε_a and ε_c are the strain at the bottom fibre of the stainless steel beam and top fibre of the concrete slab, respectively. Since the stress-stain relationship of stainless steel consists of two unique expressions (Eqs. 1 and 2 for pre- and post-yield, respectively), these, together with the compressive region in the slab, result in three different stress distributions across the cross-section, as illustrated in Fig. 2. Assuming that $y_{0.2}$ is the distance between the neutral axis (NA) and the location in the cross-section where the strain in the stainless steel section is $\varepsilon_{0.2}$, it can be determined that:

$$y_{0.2} = \frac{\varepsilon_{0.2}}{\kappa} \tag{5}$$

As presented in Fig. 2, three possible cases are considered. Case 1 is when $y_{0.2}$ is within the stainless steel web (i.e. $y_{0.2} \geq t_c - y_1 + t_f$, where y_1, t_c and t_f are the depth of the compressive area of the concrete slab, the depth of the concrete slab and the thickness of the top flange of the stainless steel section, respectively), Case 2 corresponds to the situation when $y_{0.2}$ is within the top stainless steel flange (i.e. $t_c - y_1 \leq y_{0.2} < t_c + t_f$) while in Case 3, $y_{0.2}$ is within the concrete slab (i.e. $0 < y_{0.2} < t_c - y_1$).

Based on the strain distribution and the full stainless steel stress-strain material model, the internal axial forces within the concrete slab and each individual stainless steel

component (i.e. the flanges and the web) can be calculated for all three cases. These are presented in Table 1, in which f_c is the concrete compressive strength and b_c is the width of the concrete slab acting compositely with the stainless steel section; σ_1 and σ_2 are the appropriate stresses in the stainless steel section (as defined in Eqs. 3 and 4); and b_f is the width of the stainless steel flange. The axial forces (i.e. F_{tf1}, F_{tf2}, F_{tf3}, F_{tw1}, F_{tw2} and F_c) are as defined in Fig. 2 and the corresponding moments in the section are given as M_{tf1}, M_{tf2}, M_{tf3}, M_{tw1}, M_{tw2} and M_c, respectively.

The initial step in calculating the plastic bending capacity of the composite beam is to locate the position of the neutral axis at failure (i.e. y_1). The position y_1 can be obtained based on the equilibrium of internal forces, and is given as:

$$F_{tf1} + F_{tf2} + F_{tf3} + F_{tw1} + F_{tw2} - F_c = 0 \tag{6}$$

In order to calculate the internal forces in Eq. 6 and presented in the Table 1, and hence y_1, direct integration is required. Since the internal forces depend on the variable y_1, Eq. 6 is a nonlinear problem which requires an iterative method to obtain a solution. In the current analysis, the mathematical software Matlab [33] is employed to solve these complex equations and determine the position of neutral axis. The strain at any point in the cross-section (denoted as the position y, measured from the NA) is calculated from the strain distribution and is determined as:

$$\varepsilon = \kappa\, y \tag{7}$$

where the cross-sectional curvature is obtained from:

$$\kappa = \min(\kappa_c\,, \kappa_a) \tag{8}$$

In this expression, κ_c is the limiting curvature for concrete failure (i.e. when the strain at the outer concrete fibre reaches the ultimate strain of concrete, ε_{cu}) and can be determined from:

$$\kappa_c = \varepsilon_{cu}/y_1 \tag{9}$$

The nominal ultimate strain of concrete (ε_{cu}), as a percentage, is given in Eurocode 2 [34] as:

$$\varepsilon_{cu} = 2.6 + 35[(98 - f_c)/100]^4 \text{ for } f_c \geq 50\ \text{N/mm}^2,\ \text{otherwise } 3.5 \tag{10}$$

κ_a is the limiting curvature for steel failure (i.e. when the strain at the outer steel fibre reaches the ultimate strain of stainless steel) and can be determined as:

$$\kappa_a = \frac{\varepsilon_u}{H - y_1} \tag{11}$$

where H is the overall depth of the composite beam. κ_c and κ_a define the governing failure mode of the composite member: if $\kappa_c < \kappa_a$, the composite beam fails due to concrete crushing whereas steel failure dominates when $\kappa_c > \kappa_a$.

Finally, the plastic moment capacity of the composite section (M_{pl}) can be obtained from the following expression:

$$M_{pl} = M_c + M_{tf1} + M_{tf2} + M_{tf3} + M_{tw1} + M_{tw2} \tag{12}$$

where the internal bending moments in each component of the composite cross-section are calculated with respect to the neutral axis, as presented in Table 1.

4.2.3- Simplified analytical analysis

In the previous section, an accurate analytical solution to obtain the plastic bending moment of composite stainless steel-concrete beans was presented. However, the analytical model requires numerical integration to obtain the internal forces and moments which may not be suitable for a straightforward design tool. Therefore, a simplified analytical solution is derived and proposed in the current section.

The main assumption of the simplified analytical method is that the effective area of the steel section is stressed to a constant value of σ_m, where σ_m is defined as the stress at 60% of the steel beam height, as shown in the Fig. 3. It is important to note that in Eurocode 4, the plastic bending resistance of a composite carbon steel-concrete beam is determined by assuming that the effective area of the steel member is stressed to its yield strength.

From the strain diagram in Fig. 3, it is observed that the distance between the plastic neutral axis and the location of σ_m (i.e. y_2) is determined as:

$$y_2 = t_c + 0.6\,h - y_1 \tag{13}$$

where y_1 is the height of compressive area of the concrete slab.

From horizontal equilibrium of the internal forces:

$F_c = F_t \rightarrow 0.85\, f_c\, y_1\, b_c = A_s\, \sigma_m$

or

$$y_1 = \frac{A_s}{0.85\, f_c\, b_c}\sigma_m \tag{14}$$

where A_s is the cross-sectional area of the stainless steel member.

It is assumed that $y_2 \geq y_{0.2}$, and therefore:

$$\sigma_m = \sigma_{0.2}\left[1 + \frac{r_2\left[\frac{\varepsilon_2}{\varepsilon_{0.2}} - 1\right]}{1 + (r^* - 1)\left(\frac{\frac{\varepsilon_2}{\varepsilon_{0.2}} - 1}{\frac{\varepsilon_u}{\varepsilon_{0.2}} - 1}\right)^{p^*}}\right] \tag{15}$$

in which ε_2 is the strain in the steel section at y_2 and κ is the cross-sectional curvature, determined from Eqs. 16 and 17, respectively:

$$\varepsilon_2 = \kappa\, y_2 = \kappa\,(t_c + 0.6\,h - y_1) \tag{16}$$

$$\kappa = \min(\kappa_c\,, \kappa_a) \text{ where } \kappa_c = \varepsilon_{cu}/y_1 \text{ and } \kappa_a = \frac{\varepsilon_u}{H - y_1} \tag{17}$$

Firstly, the position of the neutral axis y_1 can be determined using Eq. 14 together with Eqs. 15-17 using a trial and error technique. Finally, the plastic bending capacity of the composite beam can be calculated as:

$$M_{pl} = \sigma_m\,[H - h/2 - y_1/2] \tag{18}$$

The flow chart of the algorithm to calculate the position of the neutral axis and the bending moment capacity is shown in Fig. 4.

4.3- Partial shear connection using simplified analytical analysis

The equations presented in Section 4.2.3 to calculate the bending moment capacity of composite beams with full shear connection cannot be readily applied for composite beams with partial shear connection. However, a similar procedure can be employed to develop a new analytical solution, suitable for composite beams with partial shear connection. In these members, there are often two distinct neutral axes lying within the concrete slab and the steel section, respectively, as shown in Fig. 5 (NA-1 and NA-2 in the figure).

It can be seen from Fig. 5 that the stress distribution through the depth of the cross-section is nonlinear and therefore a complex mathematical solution is required in order to calculate the plastic bending capacity. Hence, a similar approach to that employed in the simplified analytical model proposed in Section 4.2.3 is adopted herein to predict the plastic bending moment of composite beams with a partial shear connection.

The analytical model developed in this section is based on the following assumptions:

1- The material model for stainless steel employed in the CSM is approximated using an elastic, multi-linear hardening material model, as shown in the Fig. 6. An acceptable level of accuracy can be achieved by considering six points from

the stress-strain curve of stainless steel, as shown in the figure. It worth noting that more accurate results can be achieved by considering a larger number of points from the material stress-strain response.

2- The nonlinear stress diagrams in the compressive and tensile areas of the stainless steel member are simplified to block diagrams with a constant stress value of σ_{m1} and σ_{m2} which represent the stresses at 60% of the height of the compressive and tensile areas of the steel member, respectively, measured from the neutral axis of the stainless steel member (NA-2 in Fig. 5).

3- The slip strain (ε_i) at the concrete-steel interface is assumed to be a linear function of shear connection ratio, β.

Three cases are considered, depending on the position of the second NA (NA-2 in the stainless steel section), as shown in Fig. 7. Case 1 represents the case where the second NA is within the web of the stainless steel beam element ($y_{oa} \leq h - t_f$, where h is the height of the stainless steel section and y_{oa} is the distance from NA-2 to the bottom fibre of the stainless steel section, as shown in Fig. 7), Case 2 corresponds to the situation where NA-2 is within the top flange of the stainless steel beam ($h \geq y_{oa} > h - t_f$) and Case 3 is when there is no second NA but there is still some relative displacement between the top of the stainless steel section and the concrete slab ($y_{oa} > h$).

From Fig. 7, the cross-sectional curvature at failure of the composite section is:

$$\begin{aligned} &\kappa = \min(\kappa_c, \kappa_{a1}, \kappa_{a2}) && \text{for Cases 1 and 2} \\ &\kappa = \min(\kappa_c, \kappa_{a2}) && \text{for Cases 3} \end{aligned} \tag{19}$$

where $\kappa_c = \frac{\varepsilon_{cu}}{H - y_{oc}}$; $\kappa_{a1} = \frac{\varepsilon_u}{h - y_{oa}}$; and $\kappa_{a2} = \varepsilon_u / y_{oa}$.

In these expressions, y_{oc} is the distance between the concrete NA (NA-1) and the bottom fibre of the stainless steel section, as shown in Fig. 7(a). The slip strain at the concrete-stainless steel interface (ε_s) is determined as:

$$\varepsilon_s = \varepsilon_{cb} + \varepsilon_{at} \tag{20}$$

where ε_{cb} and ε_{at} are the strains in the concrete and the steel at the interface, respectively. These can be obtained from the following expressions:

$$\varepsilon_{cb} = \kappa(y_{oc} - h) \tag{21}$$

$$\varepsilon_{at} = \kappa(h - y_{oa}) \tag{22}$$

The slip at the interface can be found using Eq. 23 [35]:

$$\varepsilon_s = (1-\beta)\left(\frac{h}{2}+\frac{t_c}{2}\right)\kappa = \alpha\,\kappa \tag{23}$$

where,

$$\alpha = (1-\beta)\left(\frac{h}{2}+\frac{t_c}{2}\right) \tag{24}$$

Substituting Eqs. 21, 22 and 23 into Eq. 20, it can be established that:

$$y_{oc} = y_{oa} + \alpha \tag{25}$$

The distances y_{m1} and y_{m2}, as indicated in Fig. 7(a), are where constant stresses are assumed, and are calculated as:

$$y_{m1} = 0.6(h - y_{oa}) \quad \text{for Case 1 and 2} \tag{26}$$

$$y_{m2} = 0.6y_{oa} \quad \text{for Case 1 and 2} \tag{27}$$

$$y_{m2} = y_{oa} - 0.4h \quad \text{for Case 3} \tag{28}$$

It is noteworthy that the distance y_{m1} is not relevant in Case 3 as the whole steel section is in compression.

The corresponding stresses at y_{m1} and y_{m2} are given by Eq. 29:

If $y_{i-1} \le y_{m1} \le y_i$

$$\sigma_{m1} = \sigma_{i-1} + E_{sh}^{i}(\kappa\, y_{m1} - \varepsilon_{i-1}) \quad \text{where } i = 1,2\ldots,6 \tag{29a}$$

If $y_{i-1} \le y_{m2} \le y_i$

$$\sigma_{m2} = \sigma_{i-1} + E_{sh}^{i}(\kappa\, y_{m2} - \varepsilon_{i-1}) \quad \text{where } i = 1,2\ldots,6 \tag{29b}$$

The strains shown in Fig. 6 are assumed to be as follows:

$$\varepsilon_0 = 0;\ \varepsilon_1 = \varepsilon_{0.2};\ \varepsilon_2 = 3\varepsilon_{0.2};\ \varepsilon_3 = 5\varepsilon_{0.2};\ \varepsilon_4 = 10\varepsilon_{0.2};\ \varepsilon_5 = 0.3\varepsilon_u\,;\varepsilon_6 = \varepsilon_u \tag{30}$$

Accordingly, the corresponding stresses can be calculated as:

$$\sigma_0 = 0$$

$$\sigma_1 = \sigma_{0.2}$$

$$\sigma_i = \sigma_{0.2}\left[1 + \frac{r_2\left[\frac{\varepsilon_i}{\varepsilon_{0.2}}-1\right]}{1+(r^*-1)\left(\frac{\frac{\varepsilon_i}{\varepsilon_{0.2}}-1}{\frac{\varepsilon_u}{\varepsilon_{0.2}}-1}\right)^{p^*}}\right] \quad i = 2,3,4,5 \tag{31}$$

$$\sigma_6 = \sigma_u$$

and E_{sh}^{i} and y_i are given as:

$$E_{sh}^{i} = \frac{\sigma_i - \sigma_{i-1}}{\varepsilon_i - \varepsilon_{i-1}} \quad i = 1,\ldots,6 \tag{32}$$

$$y_i = \varepsilon_i/\kappa \quad i = 0,1,\ldots\ldots,6 \tag{33}$$

As before, the initial step to calculate the plastic bending capacity is to locate the positions of the neutral axes at failure, y_{oa} and y_{oc}. The position y_{oa} can be obtained based on the equilibrium of horizontal forces, given as:

$$F_c + F_{cf} + F_{wc} = F_{wt} + F_{tf2} \quad \text{for Case 1} \tag{34a}$$

$$F_c + F_{cf} = F_{tf1} + F_{wt} + F_{tf2} \quad \text{for Case 2} \tag{34b}$$

$$F_c = F_{wt} \quad \text{for Case 3} \tag{34c}$$

From Fig. 7, the relationship between the internal forces and y_{oa} can be readily obtained. Substituting the resulting expression of the internal forces into Eqs 34a-c, the following equations are obtained:

$$y_{oa} = \frac{0.85 f_c b_c (H-\alpha) + (\sigma_{m1} - \sigma_{m2})(b_f - t_w) t_f + t_w \sigma_{m1} h}{0.85 f_c b_c + t_w (\sigma_{m1} + \sigma_{m2})} \quad \text{for Case 1} \tag{35a}$$

$$y_{oa} = \frac{0.85 f_c b_c (H-\alpha) + b_f h \sigma_{m1} + \sigma_{m2}(2 t_w t_f - 2 b_f t_f + b_f h)}{0.85 f_c b_c + b_f (\sigma_{m1} + \sigma_{m2}) + t_w \sigma_{m2}} \quad \text{for Case 2} \tag{35b}$$

$$y_{oa} = H - \alpha - \frac{A_s}{0.85\, f_c\, b_c} \sigma_{m2} \quad \text{for Case 3} \tag{35c}$$

Firstly, the position y_{oa} can be found using Eq. 35 together with Eqs. 26-33, by adopting a trial and error approach. Finally, the plastic bending capacity of the composite beam can be calculated by taking the moment of the internal forces about any point of the cross-section of the composite beam. The flow chart of the algorithm to calculate the position of neutral axes and the bending moment capacity is shown in Fig. 8.

5 - Development of the numerical model

There are no tests available in the literature on the flexural behaviour of composite stainless steel-concrete beams. Therefore, a numerical model is developed in the current section to examine the proposed analytical solutions. Shamass and Cashell [36] previously developed a finite-element (FE) model using the ABAQUS software for composite concrete-steel beams made from either normal or high strength materials. This numerical model was shown to be capable of accurately predicting the behaviour of composite beams in terms of bending moment capacity, initial bending stiffness and also the interaction performance for composite members with full or partial shear connections. The same numerical model is utilised herein to examine the proposed analytical solutions for stainless steel-concrete composite beams. A brief description of the model is included in the current paper and a more detailed description can be found elsewhere [36].

The model is developed using the ABAQUS finite element software [37], which is capable of achieving numerical convergence despite the geometric and material nonlinearities of the behaviour. The implicit dynamic solution method for quasi-static behaviour is employed, which provides good convergence behaviour. This method uses an implicit time integration scheme to calculate the transient dynamic or quasi-static response of a system. The flat concrete slab and steel beam are modelled using shell elements with reduced integration, namely the S4R element in ABAQUS. This element is widely used for construction applications because it provides accurate results for both thin and thick shells in an efficient manner. The shear studs are modelled using Cartesian connectors available in the ABAQUS library, which connect a node in the beam flange with a coincident node in the slab at the connector location. The nonlinear load-slip relationship of the shear connectors is modelled based on the relationship proposed by Ollgaard et al. [38]. In the present FE model, the strength of the shear connector is equal to the total compressive normal force in the concrete flange divided by the number of shear studs in the shear span (i.e. $P_{stud} = F_c/NSC$ where NSC is the number of shear connectors in the shear span). A hard contact without friction is defined between the bottom surface of concrete slab and the top surface of top flange of the steel beam. Load is applied to the beam through concentrated point loads, operated in displacement-control, at locations along the member which are defined by the user.

In terms of the material modelling, the nonlinear stress-strain relationship of concrete in compression is represented using Eq. 36, in accordance with Eurocode 2 [34]:

$$\sigma_c = \left(\frac{k\left(\frac{\varepsilon_c}{\varepsilon_{c1}}\right) - \left(\frac{\varepsilon_c}{\varepsilon_{c1}}\right)^2}{1 + (k-2)\left(\frac{\varepsilon_c}{\varepsilon_{c1}}\right)} \right) f_{cm}, \quad 0 \le \varepsilon_c \le \varepsilon_{cu1} \tag{36}$$

In this expression, ε_{cu1} is the nominal ultimate strain, ε_{c1} is the strain at the peak stress and f_{cm} is the ultimate compressive strength of concrete, given by:

$$f_{cm} = f_{ck} + 8 \tag{37}$$

where f_{ck} is the characteristic cylinder strength. The parameter k is given by:

$$k = 1.05\, E_{cm} \frac{\varepsilon_{c1}}{f_{cm}} \tag{38}$$

while E_{cm} is the elastic modulus of concrete, determined as:

$$E_{cm} = 22(0.1\, f_{cm})^{0.3} \tag{39}$$

The concrete strain at the peak stress, ε_{c1}, is obtained as a percentage as:

$$\varepsilon_{c1} = 0.7(f_{cm})^{0.31} \leq 2.8 \tag{40}$$

The nominal ultimate strain (ε_{cu1}), as a percentage, is given by:

$$\varepsilon_{cu1} = 2.8 + 27[(98 - f_{cm})/100]^4 \text{ for } f_{ck} \geq 50 \text{ N/mm}^2, \text{ otherwise } 3.5 \tag{41}$$

On the other hand, the material model for the stainless steel beam in the composite member is represented using the two-stage stress-strain relationship proposed Mirambell and Real [31] and Rasmussen [28] and described earlier in Section 4.1. The full material model is presented in Eq. 42:

$$\varepsilon = \begin{cases} \dfrac{\sigma}{E} + 0.002\left(\dfrac{\sigma}{\sigma_{0.2}}\right)^n & \text{for } 0 \leq \sigma \leq \sigma_{0.2} \\ \varepsilon_{0.2} + \dfrac{\sigma - \sigma_{0.2}}{E_2} + \varepsilon_{up}^{*}\left(\dfrac{\sigma - \sigma_{0.2}}{\sigma_u - \sigma_{0.2}}\right)^m & \text{for } \sigma_{0.2} \leq \sigma \leq \sigma_u \end{cases} \tag{42}$$

where $\varepsilon_{up}^{*} = \varepsilon_u - \varepsilon_{0.2} - \frac{\sigma_u - \sigma_{0.2}}{E_2}$ and ε and σ are the uniaxial strain and stress, respectively.

The true stress-strain curve calculated from the engineering stress-strain relationship can be calculated as follows:

$$\begin{aligned} \sigma^{true} &= \sigma(1 + \varepsilon) \\ \varepsilon^{true} &= \ln(1 + \varepsilon) \end{aligned} \tag{43}$$

6- Validation of the proposed analytical models

6.1- Full shear connection

The plastic bending capacity results obtained numerically are compared with those obtained using the full analytical analysis proposed in Section 4.2.2. Two cross-sections are used in the validation and their geometries are presented in the Table 2. The shear studs are located uniformly along the entire span of the composite beam and the total number of shear studs in the shear span is 25. Six different grades of stainless steel are used in the analysis, and their material properties are taken from Eurocode 3-Part 1-4 [23] and presented in Table 3.

Tables 4 and 5 present the bending moment capacities obtained from the numerical analysis (M_{FE}) as well as from the full and simplified analytical method ($M_{an,full}$ and $M_{an,simp}$, respectively) for beams S1 and S2. It is observed that a very good agreement is achieved between the ABAQUS and both set of analytical predictions. For beam S1, the full and simplified analytical expressions slightly underestimate the bending moment capacity in all cases but the error is always within 5%. On the other hand, for S2 which is a larger section, the full analytical model generally overestimates the capacity (all cases

except one) but only by up to 3% while the simplified analytical model generally underestimates the capacity (in all cases except one) but only by up to 2.5%. Therefore, it can be deduced that the full and simplified analytical solutions proposed in Section 4.2.2 and 4.2.3 of this paper, respectively, provide a reliable and accurate prediction of the bending moment capacity of composite beams made from stainless steel with a full shear connection.

In the following analysis, the bending moment capacity is calculated using both the full analytical analysis proposed in Section 4.2.2 and the simplified analytical expression proposed in Eq. 18. In order to examine the accuracy of the simplified analytical analysis for a wide range of the material and geometrical properties, various stainless steel grades are included in the study (austenitic, duplex and ferritic grades) as well as two different concrete strengths (C40 and C50) and different cross-section geometries, as shown in Table 6. The bending moment capacities predicted by the full analytical analysis are presented together with those obtained using the simplified expressions in Fig. 9. It can be seen that the predicted bending moment capacity obtained using the simplified analytical analysis are in very good agreement with the corresponding values obtained from the full analysis. Generally, the average deviation is within 2%. In all cases, the simplified equation predicts slightly lower values than the more detailed model but nevertheless, given the data presented in Fig. 9, it is concluded that the simplified analytical analysis developed in this study is adequate for predicting the bending strength of composite beams for specimens made from various concrete and stainless steel materials with a full shear connection. Moreover, given the significant additional complexities involved in achieving a solution for the full model compared with the straightforward solution of the simplified expressions, it is clear that the simpler expressions provide a valuable option, particularly for designers who may not have the time or expertise to solve the detailed expressions.

In order to illustrate the stress distribution through the cross-section, Fig. 10 presents these results from both the full and simplified analytical models for the composite beam with full shear connection using a S1 section in grade 1.4003 ferritic stainless steel which acts compositely with a concrete slab made from C40 concrete. It is clear that although the shape of the stress distributions through the section are quite different, the stress values at key locations are quite similar.

6.2- Partial shear connection

In Fig. 11, the bending moment capacity results obtained using finite element analysis of composite beams with partial shear connection are compared with those obtained using the analytical procedure developed in this paper. For illustration purposes, the comparison is presented for composite beam S1 with C40 concrete and grade 1.4003 stainless steel. The degree of shear connection ranges from 0.4 to 1 in the analysis. The results show a reasonable agreement between the FE and analytical prediction with the deviation between the predictions ranging between 4% and 7%. These errors are slightly larger than those presented for beams with full shear connection and this is likely to be due to the different assumptions that are made regarding the stress distribution in the cross-section. Nevertheless, Fig. 10 shows that the simplified analytical solution provides conservative bending capacity compared to the numerical results.

7 -Conclusions

Current design codes for steel-concrete composite beams neglect strain hardening of the steel member. Although this is a reasonable assumption for carbon steel, stainless steel is a very ductile material which demonstrates significant levels of strain hardening. The current research presents an adaptation of the continuous strength method (CSM) for composite beams made from stainless steel, to predict the plastic bending moment capacity for members with full and partial shear connection. Two different models are presented, namely a full, detailed model as well as a more simplified approach. Since no tests have been conducted on stainless steel-concrete composite beams, a validated finite-element model is employed to investigate the accuracy of the proposed analytical approach. The analytical analysis in the full model, in particular, requires complex mathematical solution and therefore a simplified analytical solution is also proposed, utilising the assumptions of Eurocode 4. It is concluded that both the full and simplified analytical solutions presented in this study provide an accurate prediction of the bending capacity. Moreover, the simplified analytical approach also provides a straight-forward design tool for practical engineers, which can be applied for composite beams with full or partial shear connection.

Acknowledgment

The first author would like to acknowledge the Centre for Civil and Building Services Engineering at London South Bank University for the encouragement and providing technical supports for this research.

References

[1] B. Hauke, Economic application of composite beams with moderate high strength materials. Proceedings of the 5th European Conference on Steel and Composite Structures, 2008, Graz, Switzerland.

[2] L. Gardner, X. Yun, L. Macorini, M. Kucukler, Hot-rolled steel and steel-concrete composite design incorporating strain hardening. Structures 2017, 9: 21-28.

[3] EN 1994-1-1, Eurocode 4: Design of composite steel and concrete structures — Part 1–1: General rules and rules for buildings. Brussels: European Committee for Standardization (CEN); 2005.

[4] B. Rossi, Discussion on the use of stainless steel in constructions in view of sustainability, Thin Walled Structures 2014, 83: 182-189.

[5] L. Gardner, The use of stainless steel in structures. Prog Struct Eng Mat 2005, 7: 45-55.

[6] O. Zhao, B. Rossi, L. Gardner, B. Young, Behaviour of structural stainless steel cross-sections under combined loading–Part I: experimental study. Eng Struct 2015, 89: 236-246.

[7] O. Zhao, L. Gardner, B. Young, Buckling of ferritic stainless steel members under combined axial compression and bending. J Constr Steel Res 2016, 117: 35-48.

[8] O. Zhao, L. Gardner, B. Young, Structural performance of stainless steel circular hollow sections under combined axial load and bending–Part 1: Experiments and numerical modelling. Thin Walled Struct 2016, 101: 231-239.

[9] I. Arrayago, F. Picci, E. Mirambell, E. Real, Interaction of bending and axial load for ferritic stainless steel RHS columns. Thin Walled Struct 2015, 91: 96-107.

[10] Y. Wang, L. Yang, B. Gao, Y. Shi, H. Yuan, Experimental study of lateral-torsional buckling behavior of stainless steel welded I-section beams. Int J of Steel Struct 2014, 14(2): 411-420.

[11] M. Theofanous, N. Saliba, O. Zhao, L. Gardner, Ultimate response of stainless steel continuous beams. Thin Walled Struct 2014, 83: 115-127.

[12] M. Theofanous, A. Liew, L. Gardner, Experimental study of stainless steel angles and channels in bending. Structures 2015, 4: 80-90.

[13] I. Arrayago, E. Real. Experimental study on ferritic stainless steel simply supported and continuous beams. J Constr Steel Res 2016, 119: 50-62.

[14] K.T. Ng, L. Gardner. Buckling of stainless steel columns and beams in fire. Eng Struct 2007, 29: 717-730.

[15] D. Lam, L. Gardner, M. Burdett, Behaviour of axially loaded concrete filled stainless steel elliptical stub columns. Adv in Struct Eng 2010, 13(3): 493-500.

[16] B. Uy, Z. Tao, L.H. Han, Behaviour of short and slender concrete-filled stainless steel tubular columns. J Constr Steel Res 2011, 67: 360-378.

[17] L.H Han, F. Chen, F.Y. Liao, Z. Tao, B. Uy, Fire performance of concrete filled stainless steel tubular columns. Eng Struct 2013, 56: 165-181.

[18] Z. Tao, B. Uy, F.Y. Liao, L.H. Han, Nonlinear analysis of concrete-filled square stainless steel stub columns under axial compression. J of Constr Steel Res 2011, 67: 1719-1732.

[19] M.L Patton, K.D. Singh, Finite element modelling of concrete-filled lean duplex stainless steel tubular stub columns. Int J Steel Struct 2014, 14: 619-632.

[20] L. Gardner, M. Ashraf, Structural design for non-linear metallic materials. Eng Struct 2006, 28: 926-934.

[21] L. Gardner, D.A. Nethercot, Structural stainless steel design: a new approach. J Struct Eng 2004, 82(21): 21-30.

[22] M. Ashraf, L. Gardner, D.A. Nethercot, Structural stainless steel design: resistance based on deformation capacity. J Struct Eng 2008, 134(3): 402-411.

[23] EN 1993-1-4. Eurocode 3: Design of steel structures – Part 1–4: General rules – supplementary rules for stainless steels. Brussels: European Committee for Standardization (CEN), 2006.

[24] SEI/ASCE 8-02. Specification for the design of cold-formed stainless steel structural members. Reston: American Society of Civil Engineers (ASCE); 2002.

[25] L. Gardner, The continuous strength method, Proc Inst Civ Eng Struct Build 2008, 161(3):127–33.

[26] S. Afshan, L. Gardner, The continuous strength method for structural stainless steel design. Thin Walled Struct 2013, 68: 42-49.

[27] Euro Inox/SCI. Design manual for structural stainless steel (4th edition), Building Series volume 3, Euro Inox and the Steel Construction Institute, 2017.

[28] K.J. Rasmussen, Full-range stress–strain curves for stainless steel alloys. J Constr Steel Res 2003, 59: 47-61.

[29] W. Ramberg, W.R. Osgood, Description of stress-strain curves by three parameters. Issue 902 of National Advisory Committee for Aeronautics technical note, 1943.

[30] H. Hill, Determination of stress–strain relations from offset yield strength values, Issue 927 of National Advisory Committee for Aeronautics, 1944.

[31] E. Mirambell, E. Real, On the calculation of deflection in structural stainless steel beams: an experiment and numerical investigation. J Constr Steel Res 2000, 54: 109-133.

[32] K. Abdella, Inversion of a full-range stress–strain relation for stainless steel alloys. Int J of NonLin Mech 2006, 41(3): 456-463.

[33] MATLAB version 9.1.0, The MathWorks Inc. 2016, Massachusetts, USA.

[34] EN 1992-1-1. Eurocode 2: Design of concrete structures – Part 1–1: General rules and rules for buildings. Brussels: European Committee for Standardization (CEN), 2004.

[35] H. Ban, M.A. Bradford, Elastoplastic cross-sectional behavior of composite beams with high-strength steel: analytical modelling. J Struct Eng 2014, 141(10): 04014236.

[36] R. Shamass, K.A. Cashell, Behaviour of composite beams made using high strength steel. Structures 2017, 12: 88-101

[37] Abaqus. Reference Manual, Version 6.11. France: Simulia, Dassault Systèmes, 2011.

[38] J.G. Ollgaard, R.G. Slutter, J.W. Fisher, Shear strength of stud connectors in lightweight and normal weight concrete, AISC Eng J-Canada 1971, 8: 55-64.

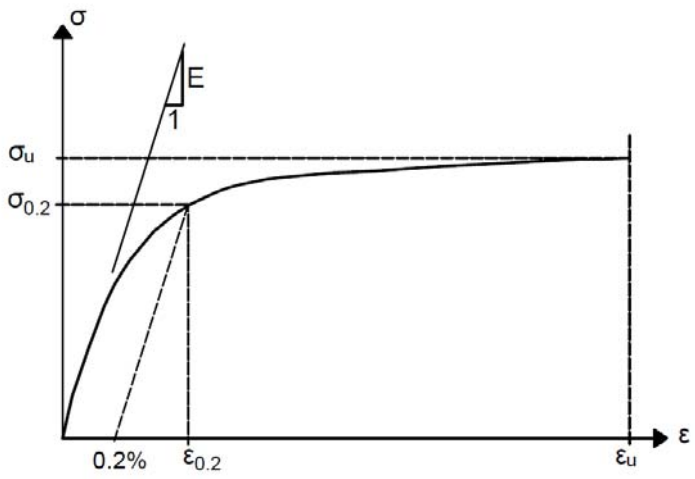

Fig. 1: Typical stress-strain relationship of stainless steel

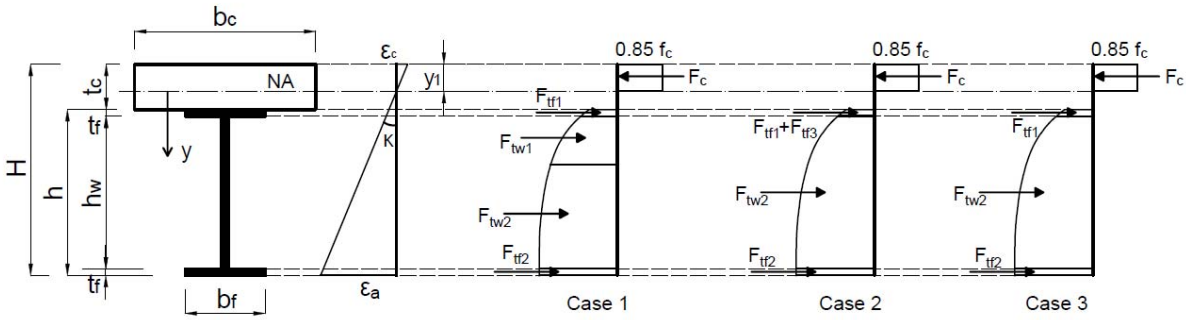

Fig. 2: The stress and strain distribution diagrams for composite beams with full shear connection

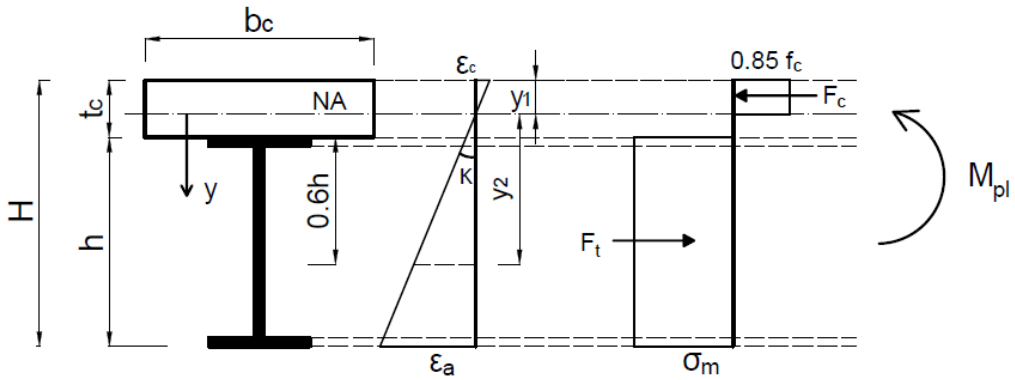

Fig. 3: The strain and stress distribution diagrams for composite beams with full shear connection based on the simplified approach

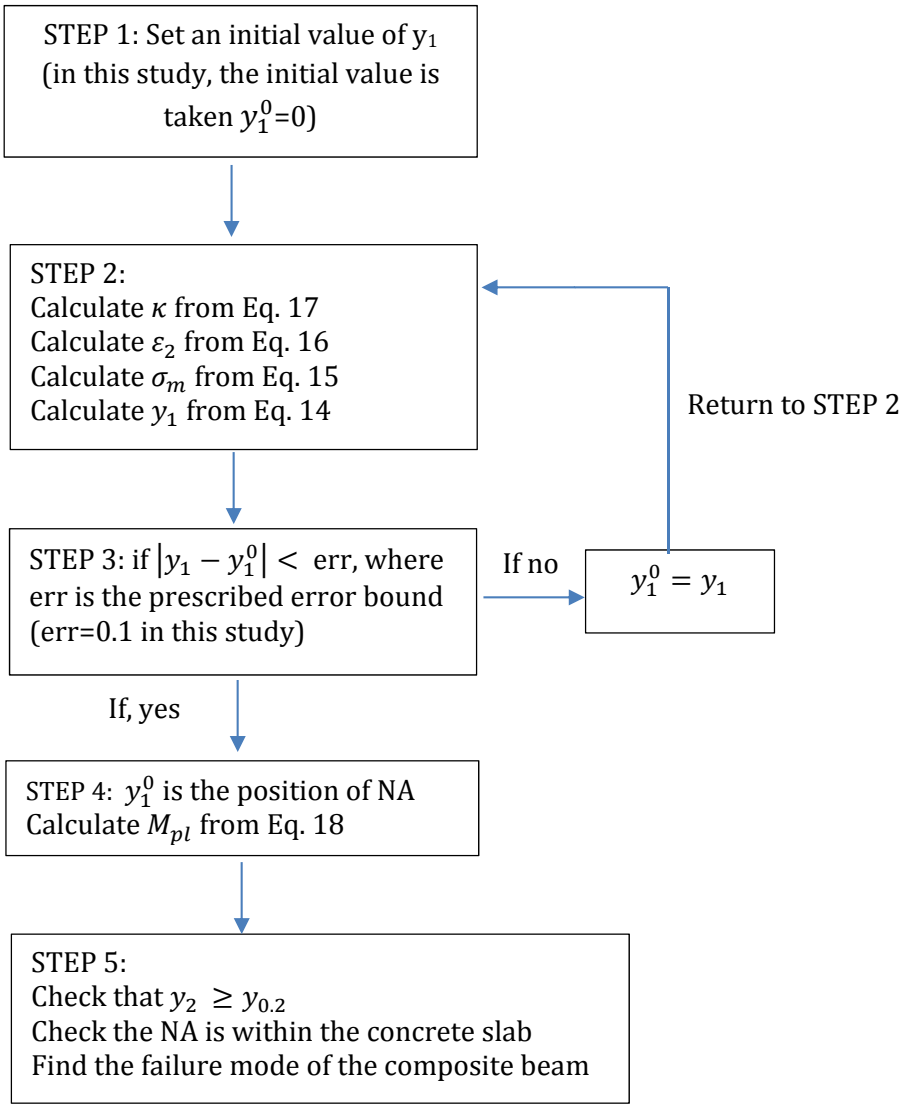

Fig. 4: Flow chart of the solution procedure

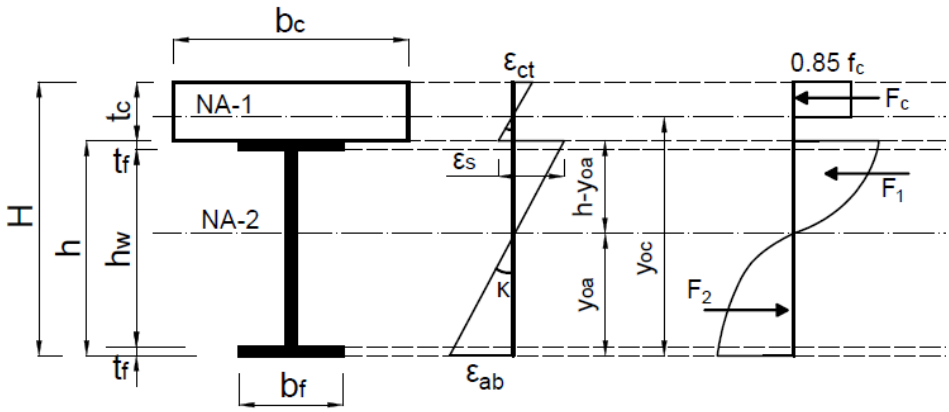

Fig. 5: The strain and stress diagram for a composite beam with partial shear connection

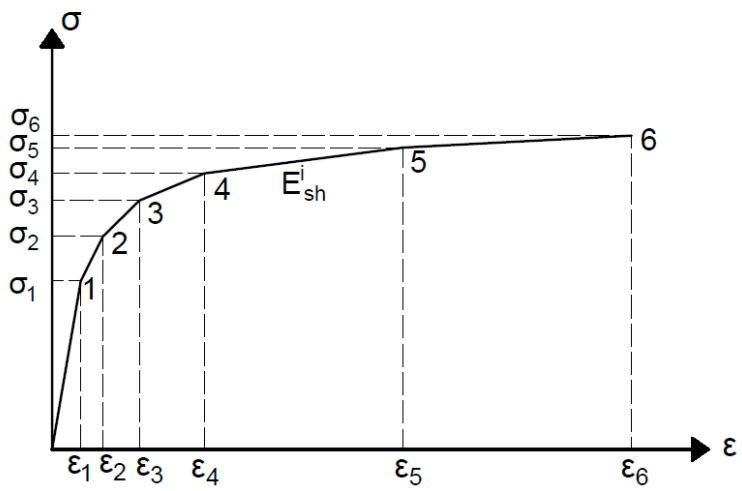

Fig. 6: CSM elastic and multi-linear hardening material model for stainless steel

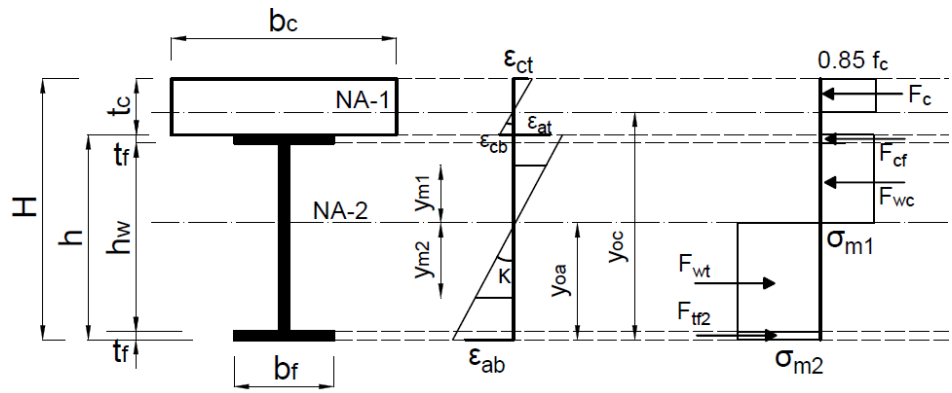

(a) Case 1: Second NA is within the steel web

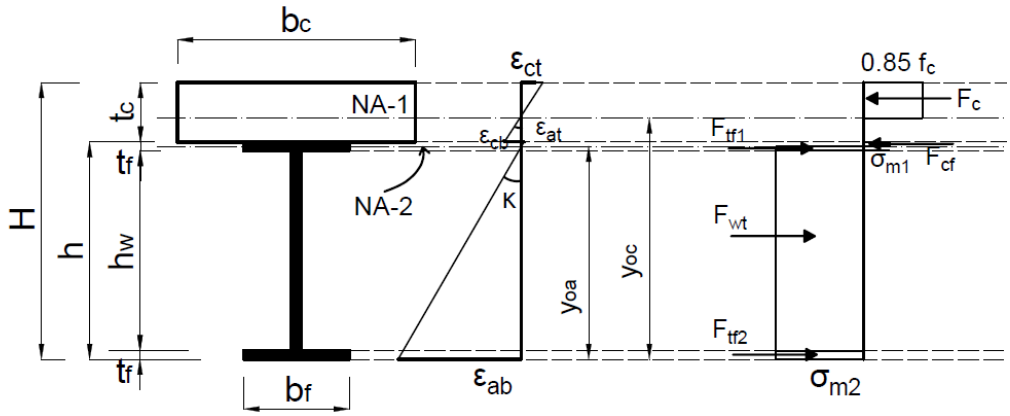

(b) Case 2: Second NA is within the steel flange

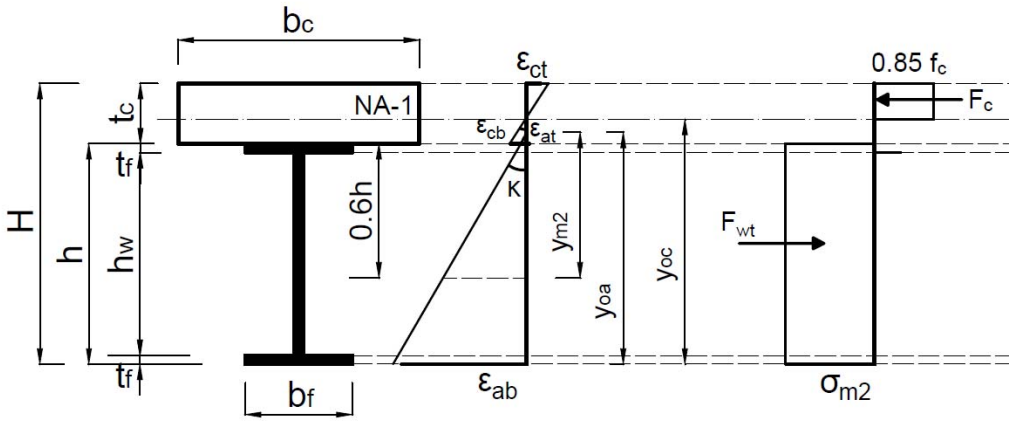

(c) Case 3: No second NA but slip strain occurs at the interface between the steel and concrete

Fig. 7: The strain and stress distribution diagrams for partial shear connection composite beams based on the simplified approach

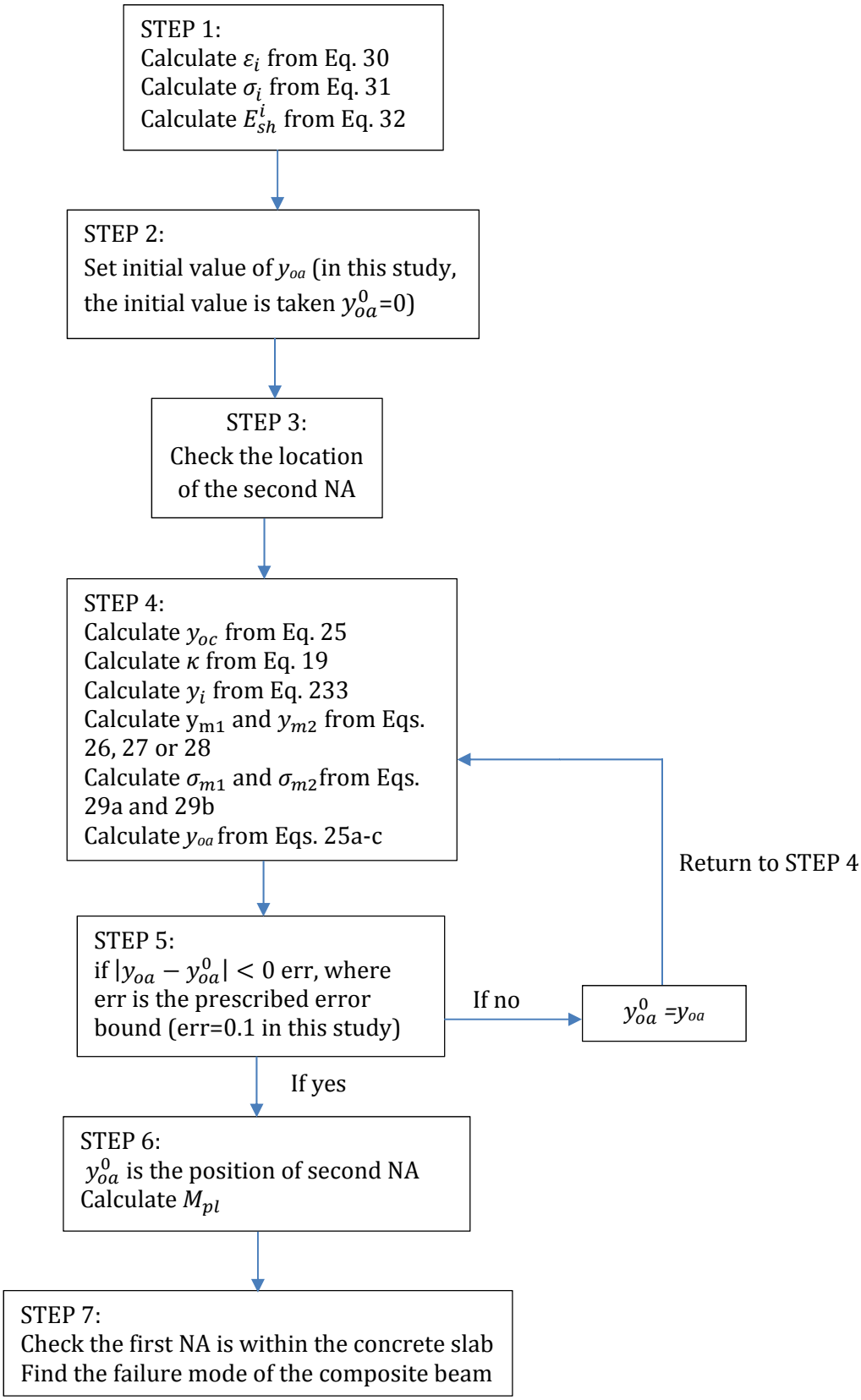

Fig. 8: Flow chart of the solution procedure

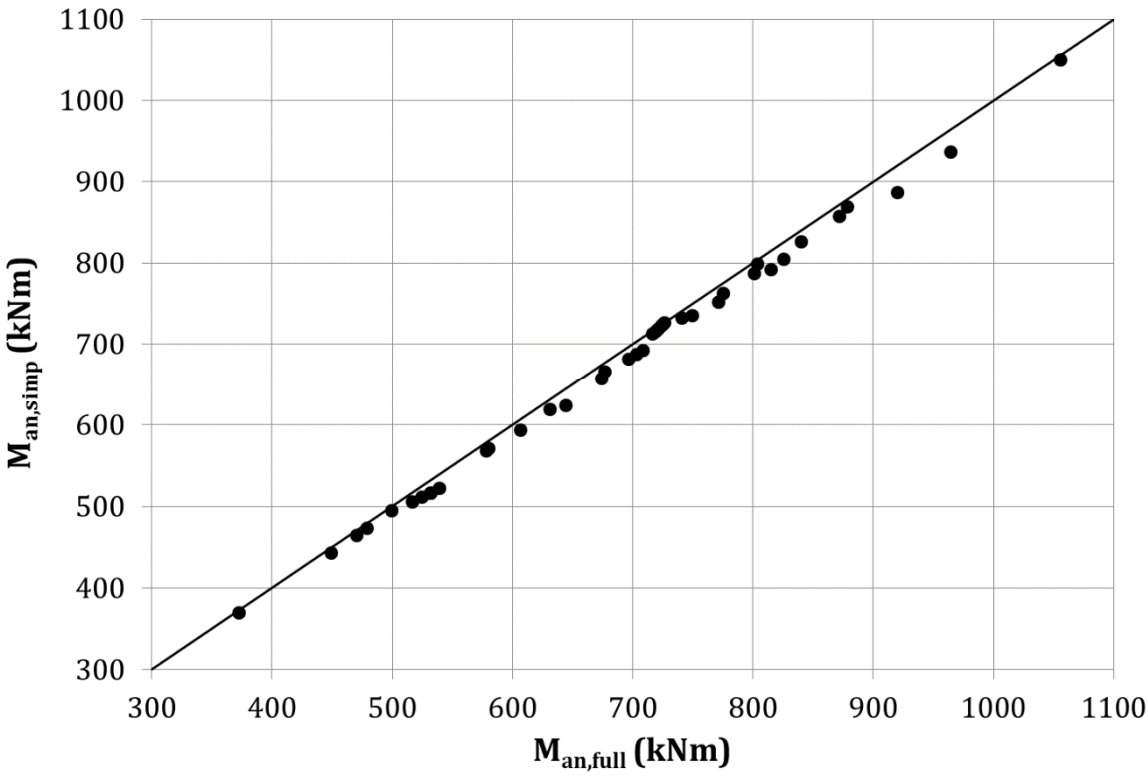

Fig. 9: Comparison between the results from the simplified and full model for composite beams with full shear connection

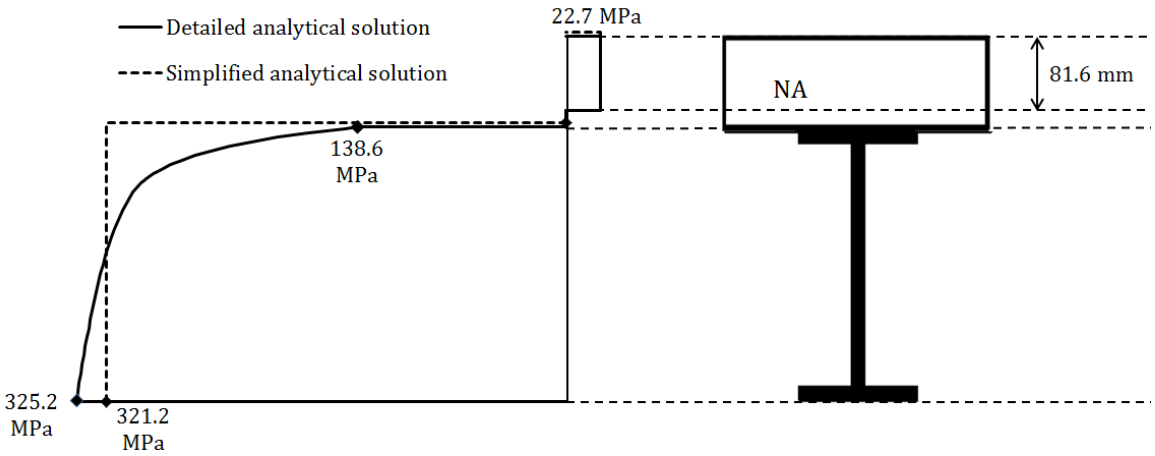

Fig. 10: The stress distribution through the cross-section of the composite beam

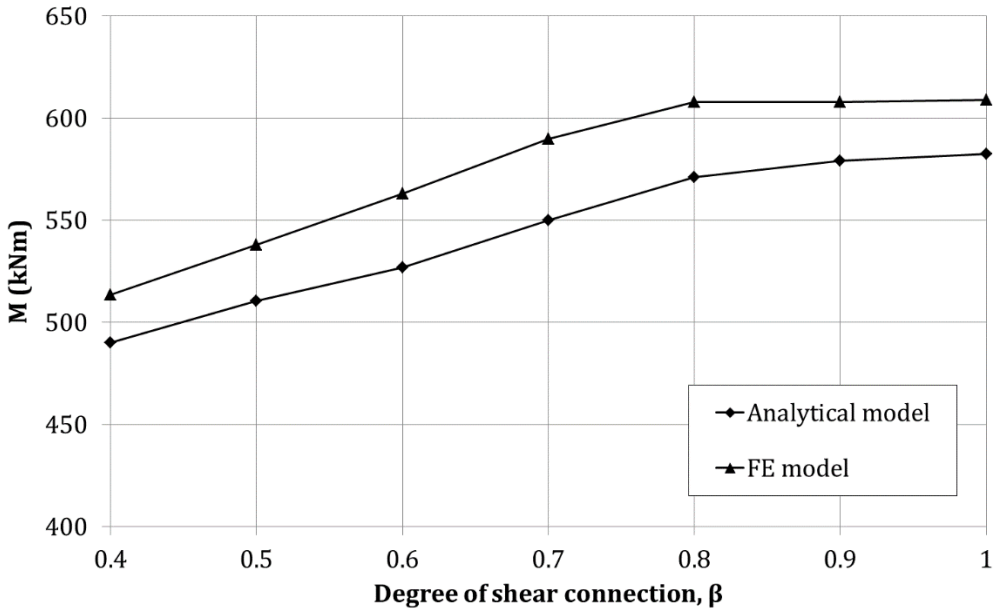

Fig. 11: Comparison between FE results and corresponding analytical results for beams with partial shear connection

Table 1: Expressions for the internal forces and bending moments in the cross-section for the three cases

	Case 1	Case 2	Case 3
F_c	$0.85\ f_c\ b_c\ y_1$	$0.85\ f_c\ b_c\ y_1$	$0.85\ f_c\ b_c\ y_1$
M_c	$0.85\ f_c\ b_c \frac{y_1^2}{2}$	$0.85\ f_c\ b_c \frac{y_1^2}{2}$	$0.85\ f_c\ b_c \frac{y_1^2}{2}$
F_{tf1}	$\int_{t_c-y_1}^{t_c-y_1+t_f} b_f\ \sigma_1(\varepsilon)\ dy$	$\int_{t_c-y_1}^{y_{0.2}} b_f\ \sigma_1(\varepsilon)\ dy$	$\int_{t_c-y_1}^{t_c-y_1+t_f} b_f\ \sigma_2(\varepsilon)\ dy$
M_{tf1}	$\int_{t_c-y_1}^{t_c-y_1+t_f} b_f\ \sigma_1(\varepsilon)\ y\ dy$	$\int_{t_c-y_1}^{y_{0.2}} b_f\ \sigma_1(\varepsilon)\ y\ dy$	$\int_{t_c-y_1}^{t_c-y_1+t_f} b_f\ \sigma_2(\varepsilon)\ y\ dy$
F_{tf2}	$\int_{H-t_f-y_1}^{H-y_1} b_f\ \sigma_1(\varepsilon)\ dy$	$\int_{H-t_f-y_1}^{H-y_1} b_f\ \sigma_2(\varepsilon)\ dy$	$\int_{H-t_f-y_1}^{H-y_1} b_f\ \sigma_2(\varepsilon)\ dy$
M_{tf2}	$\int_{H-t_f-y_1}^{H-y_1} b_f\ \sigma_1(\varepsilon)\ y\ dy$	$\int_{H-t_f-y_1}^{H-y_1} b_f\ \sigma_2(\varepsilon)\ y\ dy$	$\int_{H-t_f-y_1}^{H-y_1} b_f\ \sigma_2(\varepsilon)\ y\ dy$
F_{tf3}	-----	$\int_{y_{0.2}}^{t_c-y_1+t_f} t_w\ \sigma_2(\varepsilon)\ dy$	-----
M_{tf3}	-----	$\int_{y_{0.2}}^{t_c-y_1+t_f} t_w\ \sigma_2(\varepsilon)\ y\ dy$	-----
F_{tw1}	$\int_{t_c-y_1+t_f}^{y_{0.2}} t_w\ \sigma_1(\varepsilon)\ dy$	-----	-----
M_{tw1}	$\int_{t_c-y_1+t_f}^{y_{0.2}} t_w\ \sigma_1(\varepsilon)\ y\ dy$	-----	-----
F_{tw2}	$\int_{y_{0.2}}^{H-t_f-y_1} t_w\ \sigma_2(\varepsilon)\ dy$	$\int_{t_c-y_1+t_f}^{H-t_f-y_1} t_w\ \sigma_2(\varepsilon)\ dy$	$\int_{t_c-y_1+t_f}^{H-t_f-y_1} t_w\ \sigma_2(\varepsilon)\ dy$
M_{tw2}	$\int_{y_{0.2}}^{H-t_f-y_1} t_w\ \sigma_2(\varepsilon)\ y\ dy$	$\int_{t_c-y_1+t_f}^{H-t_f-y_1} t_w\ \sigma_2(\varepsilon)\ y\ dy$	$\int_{t_c-y_1+t_f}^{H-t_f-y_1} t_w\ \sigma_2(\varepsilon)\ y\ dy$

Table 2: Geometry of the composite beams used for the validation study

Section name	b_c (mm)	t_c (mm)	t_w (mm)	h (mm)	b_f (mm)	t_f (mm)
S1	1200	100	10.2	304.8	152.4	18.2
S2	1500	100	12	400	190	18.2

Table 3: Material properties of stainless steel [23]

Type of stainless steel	Grade	$\sigma_{0.2}$ (N/mm²)	σ_u (N/mm²)	n	A (%)
Ferritic	1.4003	280	450	7	51
	1.4016	260	450	6	38
	1.4512	210	380	9	44
Austenitic	1.4571	220	520	7	40
	1.4406	280	580	8	40
Duplex	1.4362	400	630	5	20

Table 4: Comparison between the numerical and analytical bending moment for the beam S1

Stainless steel grade	Concrete grade	FE bending moment capacity, M_{FE} (kNm)	Full analytical bending moment capacity, $M_{an,full}$ (kNm)	Simplified analytical bending moment capacity, $M_{an,simp}$ (kNm)	$\frac{M_{an,full}}{M_{FE}}$ (%)	$\frac{M_{an,simp}}{M_{FE}}$ (%)
1.4003	C40	606.5	588.9	584	-2.9	-3.7
1.4016	C40	585.0	565.6	559	-3.3	-4.4
1.4512	C40	493.0	476.3	470.5	-3.4	-4.6
1.4571	C50	567.0	549.9	538.6	-3.0	-5
1.4406	C50	664.0	643.7	632.2	-3.1	-4.8
1.4362	C50	836.5	828.0	818.5	-1.0	-2.2

Table 5: Comparison between the numerical and analytical bending moment for the beam S2

Stainless steel grade	Concrete grade	FE bending moment capacity, M_{FE} (kNm)	Full analytical bending moment capacity, $M_{an,full}$ (kNm)	Simplified analytical bending moment capacity, $M_{an,simp}$ (kNm)	$\frac{M_{an,full}}{M_{FE}}$ (%)	$\frac{M_{an,simp}}{M_{FE}}$ (%)
1.4003	C40	967.2	977.23	965	1.0	-0.2
1.4016	C40	930.0	939.1	925	1.0	-0.5
1.4512	C40	791.0	789.2	777	-0.2	-1.8
1.4571	C50	913.0	916.0	892	0.3	-2.3
1.4406	C50	1058.1	1062.0	1047	1.0	-1.05
1.4362	C50	1330.0	1370.0	1346	3.0	1.2

Table 6: Range of material and geometrical parameters used in the comparison

n	$\sigma_{0.2}$ (MPa)	σ_u (MPa)	f_c (MPa)	b_c (m)	h (mm)	b_f (mm)	t_c (mm)
5-21	200-400	500-660	30-50	1.0-3.0	150-400	100-250	80-200